Redox Behavior of Magnetite: Implications for Contaminant Reduction

CHRISTOPHER A. GORSKI,[†] JAMES T. NURMI,[‡] PAUL G. TRATNYEK,[‡] THOMAS B. HOFSTETTER,[§] AND MICHELLE M. SCHERER*,[†]

Civil and Environmental Engineering, University of Iowa, Iowa City, Iowa 52240, Division of Environmental and Biomolecular Systems, Oregon Health & Science University, Beaverton, Oregon 97006, and Institute of Biogeochemistry and Pollutant Dynamics, Swiss Federal Institute of Technology (ETH), Zurich, Switzerland

Received June 11, 2009. Revised manuscript received September 29, 2009. Accepted September 30, 2009.

The factors controlling rates of contaminant reduction by magnetite (Fe_3O_4) are poorly understood. Here, we measured the reduction rates of three $ArNO_2$ compounds by magnetite particles ranging from highly oxidized ($x = Fe^{2+}/Fe^{3+} = 0.31$) to fully stoichiometric ($x = 0.50$). Rates of $ArNO_2$ reduction became almost 5 orders of magnitude faster as the particle stoichiometry increased from $x = 0.31$ to 0.50. To evaluate what was controlling the rate of $ArNO_2$ reduction, we measured apparent ^{15}N kinetic isotope effects (^{15}N-AKIE) values for nitrobenzene and magnetite open-circuit potentials (E_{OCP}). ^{15}N-AKIE values were greater than unity for all magnetite stoichiometries investigated, indicating that mass transfer processes are not controlling the rate of $ArNO_2$ reduction by magnetite. E_{OCP} measurements showed that the E_{OCP} for magnetite was linearly related to the stoichiometry, with more stoichiometric magnetite having a lower potential. Based on these results, we propose that conceptual models that incorporate both redox and Fe^{2+} diffusion processes, rather than those that rely solely on diffusion of Fe^{2+}, are more appropriate for understanding contaminant reduction by magnetite. Our work indicates that particle stoichiometry should be considered when evaluating rates of contaminant reduction by magnetite.

Introduction

Magnetite (Fe_3O_4) is a common constituent of soils and sediments (*1, 2*). Magnetite can form naturally via several pathways including iron metal corrosion (*3*), Fe^{2+} oxidation (*1*), and chemical and biological reduction of Fe^{3+} oxides (*4, 5*). Due to the ubiquity of magnetite in the environment, it has been implicated as a potentially important reductant for environmental contaminants, including several halogenated organics and heavy metals (e.g., *4, 6*−*8*). Magnetite is also of great interest to the corrosion community, as it is a common oxidation product of steel (e.g., *3*).

We have previously demonstrated that the degree of magnetite oxidation, measured as the ratio of structural Fe^{2+} and Fe^{3+} atoms ($x = Fe^{2+}/Fe^{3+}$), strongly influences the rate of nitrobenzene ($ArNO_2$) reduction (*9*). The extent of magnetite oxidation, or magnetite stoichiometry (x), can range from 0 to 0.5, where 0.5 corresponds to the most reduced form (stoichiometric magnetite), and 0 is the completely oxidized form (all Fe^{3+}), which is known as maghemite (γ-Fe_2O_3). In our previous work, we observed that stoichiometric magnetite could rapidly reduce $ArNO_2$ in the absence of dissolved Fe^{2+}, whereas reduction by partially oxidized magnetite was much slower; however, the factors controlling the rate of $ArNO_2$ reduction and magnetite oxidation were unclear.

Several models have been proposed to describe the kinetics of magnetite oxidation, with many derived from corrosion studies where magnetite and maghemite form passive films on iron metal (*10*−*15*). Models based on diffusion of Fe^{2+} outward to the magnetite surface (*10*−*13*) are the most common, and have been invoked to explain carbon tetrachloride (CCl_4) reduction by magnetite (*16*). Although diffusion models can often describe the data well, the room temperature diffusion rates for Fe^{2+} estimated from these models vary by several orders of magnitude among studies (10^{-3} cm^2 s^{-1} (*10*), 10^{-12} to 10^{-16} cm^2 s^{-1} (*11*), 2.1×10^{-15} cm^2 s^{-1} (*12*), $1.3 \times 10^{\times 20}$ cm^2 s^{-1} (*13*)), raising questions about the assumption of diffusion control on rates of magnetite oxidation (*14, 17, 18*). Others have proposed alternative models based on changes in magnetite redox potential upon oxidation (*14, 15*), and evidence for these models has been accumulating based on direct measurements of magnetite redox potentials upon oxidation (*8, 15, 19*).

To explore whether $ArNO_2$ reduction by oxidized magnetite is controlled by changes in the redox potential of the particle or by diffusion of Fe^{2+} to the magnetite surface, we measured the apparent ^{15}N kinetic isotope effects (^{15}N-AKIE) for $ArNO_2$ reduction and open-circuit potentials as a function of magnetite stoichiometry. We purposefully minimized the variation in specific surface areas among the batches of magnetite (~20 nm spheres, 63 ± 7 m^2 g^{-1}) in an attempt to isolate the influence of magnetite stoichiometry as the sole variable. $ArNO_2$ and its substituted analogs (3-Cl-$ArNO_2$, 2-Me-$ArNO_2$) were selected as model environmental contaminants due to the extensive body of knowledge available regarding their reactivity and substituent-dependent redox properties (*20*−*24*). We further apply this model to develop a quantitative structure−activity relationship (QSAR) that may be useful for predicting rates of $ArNO_2$ reduction, and perhaps even other environmentally relevant contaminants.

Experimental Section

Magnetite Synthesis and Characterization. Details regarding the chemicals and instrumentation used can be found in the Supporting Information (SI). Magnetite batches were synthesized using methods to control particle size and stoichiometry; a detailed explanation of the synthesis can be found in our previous work (*9*). Briefly, magnetite was synthesized in a H_2/N_2 (6/94) anaerobic glovebox by mixing a 1:2 Fe^{2+}:Fe^{3+} acidic solution, with the pH titrated to at least 10 with NaOH. H_2O_2 was used to oxidize the stoichiometric magnetite to produce oxidized magnetite powders, and x was determined by complete dissolution in acid with $\sigma_x < 0.01$ (*9*).

Mössbauer spectroscopy and powder X-ray diffraction (pXRD) patterns indicated magnetite as the sole phase present, as shown in our previous work (*9*). BET specific surface areas (SSAs) were 59 m^2 g^{-1} ($x = 0.50$), 66 m^2 g^{-1}

* Corresponding author e-mail: michelle-scherer@uiowa.edu.
[†] University of Iowa.
[‡] Oregon Health & Science University.
[§] Swiss Federal Institute of Technology (ETH).

10.1021/es9016848
Published on Web 10/13/2009

($x = 0.49$), 58 $m^2\ g^{-1}$ ($x = 0.48$), 75 $m^2\ g^{-1}$ ($x = 0.42$), 64 $m^2\ g^{-1}$ ($x = 0.36$), and 58 $m^2\ g^{-1}$ ($x = 0.31$), with the average SSA being $63 \pm 7\ m^2\ g^{-1}$. The SSAs were not measured for the $x = 0.33$, 0.22, and 0.17 batches, but TEM images indicated particle sizes similar to the $x = 0.36$ batch from which they were synthesized. pXRD patterns also provided similar primary crystallite sizes ($\sim 11 \pm 1$ nm) for all measured batches using the Scherrer equation. Transmission electron microscopy (TEM) images showed particles having spherical morphologies with diameters of approximately 20 nm (*9*); there was no evidence of any distinct phase separation (i.e., a core−shell structure).

Nitrobenzene Reduction Experiments. Reduction rates of three $ArNO_2$ compounds were investigated, including 3-Cl-nitrobenzene (3-Cl-$ArNO_2$, $E_h^{1'} = -0.405$ V), nitrobenzene ($ArNO_2$, $E_h^{1'} = -0.485$ V), and 2-methyl-nitrobenzene (2-Me-$ArNO_2$, $E_h^{1'} = -0.590$ V) (*20*). All experiments were conducted in an anaerobic H_2/N_2 (6/94) glovebox measuring less than 1 ppm oxygen. For these experiments, 1.0 ± 0.07 g/L magnetite was added to a solution containing 50 mM 3-(*N*-morpholino)propanesulfonic acid buffer (MOPS, pK_a 7.2) adjusted to pH 7.2, and allowed to equilibrate 1 hour prior to the addition of a methanolic $ArNO_2$ stock to achieve a final concentration of 40 μM $ArNO_2$; the MeOH concentration was approximately 50 mM. All reactors were run in duplicate, with reported rates being the average of the two experiments; agreement was generally within 10−15%. Samples were taken at time intervals by filtering the solution through an 0.2-μm PTFE filter, and measuring the aqueous concentration using high-pressure liquid chromatography (HPLC) with an eluent of 70:30 acetonitrile:1 g/L ammonium acetate in water (pH ≈ 7) passed through a Supelco LC-18 column at 1 mL/min. All $ArNO_2$ and aniline compounds were measured using UV absorbance detection at 254 and 235 nm, respectively.

Electrochemistry. Chronopotentiograms (CPs) of the open-circuit potential (E_{OCP}) were obtained in a two-electrode cell, containing a powder disk electrode (PDE) made with the synthesized magnetite samples and a Ag/AgCl reference electrode (values converted to SHE). Details of the design and electrochemical properties of the PDE used in this study have been published previously (*25, 26*). Custom caps (Teflon or Kel-F) were used to cover the tip of a polished disk electrode made with high purity Fe^0, leaving a 1.4 mm diameter × 5.1 mm deep cavity that was filled by pressing the sample into the cavity with a small metal plunger (this compression was sufficient to hold sample in the cavity). All results presented here were obtained with a stationary PDE. Electrode potentials were recorded with a potentiostat (Autolab PGSTAT30; EcoChemie, Utrecht, The Netherlands) without built-in resistance compensation. The sampling rate for chronopotentiometry was 2.0 s^{-1}. Linear sweep voltammetry (LSV) was also used to characterize the samples, but irreversible redox reactions occurred during the sweep, similar to previous observations on magnetite electrodes (*11*).

Nitrobenzene Stable Isotope Analysis. Nitrogen isotope fractionation associated with the reduction of $ArNO_2$ was examined in suspensions of 6.0 ± 0.07 g/L magnetite and 400 μM initial $ArNO_2$ concentrations under conditions otherwise identical to those described above ([MeOH] = 12 mM). Magnetite stoichiometries (x) examined were 0.36, 0.42, 0.49, and 0.50. For each experiment (i.e., magnetite stoichiometry) up to 7 individual reactors were prepared. Nitrogen isotope signatures of $ArNO_2$ at different extent of reactant conversion were obtained from compound-specific isotope analysis (CSIA). Following a procedure described earlier, individual reactors were sacrificed for solid-phase microextraction (SPME) and subsequent isotope analysis by GC/C/IRMS (gas chromatography isotope-ratio mass spectrometry with combustion interface) (*27, 28*).

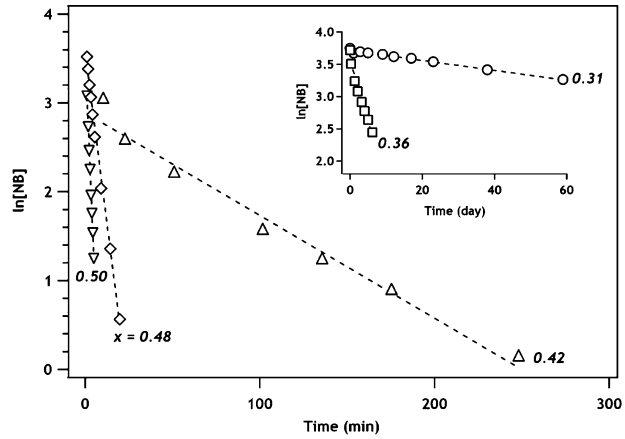

FIGURE 1. First-order plot for $ArNO_2$ reduction by magnetite with different stoichiometries ($x = Fe^{2+}/Fe^{3+}$). Legend: ▽ x = 0.50, ◇ x = 0.48, △ x = 0.42, □ x = 0.36, ○ x = 0.31. Experimental conditions: 1.0 g/L magnetite, pH 7.2, 50 mM MOPS buffer, 1 h equilibration prior to addition of $ArNO_2$, $[ArNO_2]_0 = 40\ \mu M$.

All $\delta^{15}N$ values were derived from triplicate measurements and are reported relative to N_2 in air as $\delta^{15}N_{Air}$. All samples were diluted to the least concentrated nitrobenzene solution prior to analysis and measured at constant peak amplitudes (*24*). Bulk ^{15}N enrichment factors (ε_N) of the $ArNO_2$ were derived from linear regression analysis of eq 1.

$$\ln\left[\frac{\delta^{15}N_0 + \Delta\delta^{15}N_0 + 1000}{\delta^{15}N_0 + 1000}\right] = \frac{\varepsilon_N}{1000} \cdot \ln\left(\frac{c}{c_0}\right) \qquad (1)$$

where $\delta^{15}N_0$ is the initial ^{15}N signatures of $ArNO_2$ ($-3.96 \pm 0.48‰, \pm 1\sigma$), $\Delta\delta^{15}N$ is its change during the reaction, and c_0 and c are the substrate's initial concentration and concentration following different extents of $ArNO_2$ reduction, respectively. Apparent ^{15}N kinetic isotope effects (^{15}N-AKIE) were calculated according to eq 2.

$$^{15}N - AKIE = \left(\frac{1}{1 + {}^{\varepsilon_N}/_{1000}}\right) \qquad (2)$$

Results and Discussion

Reduction of Substituted Nitrobenzene Compounds by Magnetite. We previously reported that the stoichiometry, or Fe^{2+}/Fe^{3+} ratio of magnetite (x), strongly influenced the kinetics of $ArNO_2$ reduction to aniline ($ArNH_2$) (*9*). Here, we further explored this by synthesizing several batches of magnetite with bulk stoichiometries ranging from $x = 0.50$ (stoichiometric) to $x = 0.17$ (significantly oxidized). Figure 1 shows a first-order plot for the reduction of $ArNO_2$ by 5 batches of magnetite with different stoichiometries. $ArNO_2$ reduction rates become slower as the magnetite becomes more oxidized (decreasing x). For the stoichiometric magnetite ($x = 0.50$), the half-life of $ArNO_2$ is approximately 1 minute, whereas for the most oxidized magnetite ($x = 0.31$), the half-life is approximately 3 months. Mass balances ranged between 98 and 104% based on formation of the aniline product, as shown in Figure 2 for $x = 0.42$. Note that experiments with more oxidized magnetite ($x = 0.26$) were conducted, but the reduction rate was too slow to obtain a reliable rate estimate over a 4-month time period. Slower rates of contaminant reduction by oxidized magnetite are consistent with earlier studies examining chromate reduction, where magnetite exposed to air for various time periods (i.e., months) slowed chromate reduction rates (*29*). These observations also agree with decreasing rates of $ArNO_2$ and chlorohydrocarbon reduction by structural Fe^{2+} in smectite

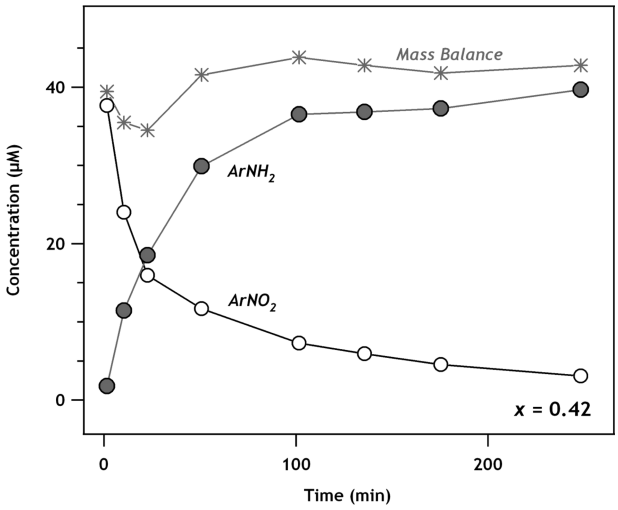

FIGURE 2. Reduction of $ArNO_2$ to $ArNH_2$ by $x = 0.42$ magnetite with the mass balance of $ArNO_2$ and $ArHN_2$ shown. Experimental conditions: 1.0 g/L magnetite, pH 7.2, 50 mM MOPS buffer, 1 h equilibration prior to addition of $ArNO_2$, $[ArNO_2]_0 = 40\ \mu M$.

minerals with decreasing Fe^{2+}-content in the octahedral clay sheets and decreasing Fe^{2+}/Fe^{3+} ratios (*30, 31*).

A similar trend of faster reduction rates with increasing magnetite stoichiometry was observed for two substituted $ArNO_2$ compounds (Figures S1−S3). As expected based on their one-electron potentials ($E_h^{1'}$), 3-Cl-$ArNO_2$ was reduced the fastest with a one-electron potential of $E_h^{1'} = -0.405$ V, followed by $ArNO_2$ ($E_h^{1'} = -0.485$ V), and 2-Me-$ArNO_2$ ($E_h^{1'} = -0.590$ V) for all stoichiometries (Table 1). Comparison of reduction rates with existing work is difficult because the stoichiometry of magnetite is not reported in previous studies. As we noted in our previous work (*9*), we suspect that differences in magnetite stoichiometry can explain discrepancies in contaminant reduction rates found among earlier studies (e.g., CCl_4) (*16, 32*).

A plot of the natural log of the first-order rate coefficient (k_{obs}) versus x reveals a linear correlation (Figure 3; $R^2 = 0.96$ for regression of all of the compounds together, and $R^2 \geq 0.97$ for the individual compounds). Substituent effects on reduction rates are much less pronounced than the effect of stoichiometry, and only span up to about 1 order of magnitude, in comparison to the 5 orders of magnitude range observed as a function of magnetite stoichiometry (Table 1). In addition, the substituent effects appear to become more significant as the magnetite becomes more oxidized (x decreases); this is shown by the markers becoming more vertically spread out with smaller x values, which indicates a possible shift in the rate-limiting step.

Nitrobenzene Stable Isotope Analysis. To evaluate whether the rate-limiting step in $ArNO_2$ reduction was shifting with magnetite stoichiometry, we determined apparent ^{15}N kinetic isotope effects (^{15}N-AKIE, eq 2) by measuring the enrichment of ^{15}N over the course of a reduction experiment. As found previously for solid-phase Fe^{2+} species (*30, 31*), ^{14}N in $ArNO_2$ is preferentially reduced, which leads to ^{15}N enrichment in the remaining $ArNO_2$, as observed in increasing $\delta^{15}N$ signatures (data not shown). Figure 4 shows that N isotope fractionation during $ArNO_2$ reduction was substantial, and most pronounced for $x = 0.36$. The magnitude of isotope fractionation, as quantified by its ^{15}N enrichment factors, ϵ_N (eq 1), decreased with increasing rates of $ArNO_2$ reduction, and thus, with increasing stoichiometry (x) of magnetite. The corresponding ^{15}N-AKIE values were between 1.0176 ± 0.0007 ($x = 0.50$) and 1.0481 ± 0.0016 ($x = 0.36$) (Table 1). Note that transport processes, such as diffusion, only lead to negligible isotope fractionation; therefore, ^{15}N-AKIE values significantly different from unity for all magnetite stoichiometries rule out that mass-transfer processes fully governed the reaction kinetics of $ArNO_2$ reduction.

Experimental and computational evidence for nitroaromatic compound reduction by a variety of dissolved and mineral bound reductants imply that ^{15}N kinetic isotope effects greater than 1.03 are typical for reaction kinetics that are limited by the cleavage of the first N−O bond of substituted *N,N*-dihydroxyanilines after sequential transfer of electrons and protons to the Ar-NO_2 ($e^-/H^+/e^-/H^+$-pathway) (*24, 27*). The ^{15}N-AKIE of 1.048 and 1.041 for more oxidized magnetite samples ($x = 0.36$ and 0.42) are both greater than 1.03, and suggest that $ArNO_2$ reduction was limited by cleavage of the first N−O bond, not electron and proton transfers to the $ArNO_2$, nor by transport processes of aqueous $ArNO_2$ to the particle surface.

The decrease of ^{15}N isotope effects by 50% and more found for the more stoichiometric magnetites ($x = 0.49$ and 0.50) suggests that either a nonisotopic transport process, such as migration of Fe^{2+} outward to the magnetite surface or diffusion of $ArNO_2$ to the magnetite surface, may be masking the isotope fractioning bond cleavage, or a change in the initial reaction mechanism may be occurring. The fast reaction kinetics (half-life ≈ 1 min) suggests a nonisotropic transport process (i.e., diffusion of $ArNO_2$ to a reactive site or solid state Fe^{2+} migration) may be responsible for the lack of fractioning bond cleavage. Shifts in ^{15}N-AKIE with increasing rates of nitroaromatic compound reduction in homogeneous solution have recently been observed due to changes in the initial reaction mechanisms. At more negative reduction potentials and under proton-limited conditions, substantially lower ^{15}N-AKIE values have been reported (*24* and refs therein), which have been attributed to the second electron transfer to the nitroaromatic radical anion becoming the rate-limiting step. Thus, ^{15}N-AKIE of 1.0235 ± 0.0008 ($x = 0.49$) and 1.0176 ± 0.0007 ($x = 0.50$) could also indicate that at least some of the $ArNO_2$ reduction at stoichiometric magnetite particles occurs via an $e^-/e^-/H^+/H^+$-pathway instead of the $e^-/H^+/e^-/H^+$-sequence. This interpretation of $ArNO_2$ reduction kinetics would require that for $x = 0.49$ and 0.50, some Fe^{2+} species have a more negative reduction potential than in partially oxidized magnetite.

Open Circuit Potential of Magnetite as a Function of Stoichiometry. To estimate redox potentials of magnetite as a function of stoichiometry, we used a powder disk electrode (PDE) to measure the self-induced potential, which is more commonly referred to as the open circuit potential (E_{OCP}). Powder electrode configurations have previously been used for characterizing the electrochemical properties of Fe^0 powders (*26*), goethite (α-FeOOH) (*33*), and other oxides (*34* and refs therein). Chronopotentiometric (CP) experiments were conducted where E_{OCP} values were measured without any applied potential for a 60-min period for 9 batches of magnetite with varied stoichiometries (Table S1 and Figure S4). The limiting value of E_{OCP} at 60 min varied linearly over more than 500 mV (−0.48 V to + 0.05 V vs SHE) as magnetite stoichiometry decreased from 0.5 to 0.17 (Figure 5). Stoichiometric magnetite had the lowest reduction potentials consistent with the faster nitroaromatic reduction rates shown in Figure 1 and the shift to lower ^{15}N-AKIE values shown in Figure 4. Both the magnitudes and trend of E_{OCP} values as a function of magnetite oxidation are consistent with previous studies conducted with magnetite single crystals (*11, 19*). Note, however, that there is a wide range of measured magnetite redox potentials reported in the literature (e.g., at neutral pH: +0.66 V (*35*), +0.25 V (*11*),

TABLE 1. First-Order Rate Coefficients (k_{obs}, min^{-1}), $t_{1/2}$ (min), LFER Slope, and ^{15}N-AKIE of $ArNO_2$ Reduction for Different Stoichiometry Magnetites (x)

		k_{obs} (min^{-1})[b]					
compound	$E_h^{1'}$[a](V)	$x = 0.50$[c]	$x = 0.49$[d]	$x = 0.48$	$x = 0.42$	$x = 0.36$	$x = 0.31$
3-Cl-$ArNO_2$	−0.405	0.74	0.29	0.29	5.8×10^{-2}	3.4×10^{-4}	3.4×10^{-5}
$ArNO_2$	−0.485	0.57	0.16	0.20	9.4×10^{-3}	1.3×10^{-4}	5.4×10^{-6}
2-Me- $ArNO_2$	−0.590	0.43	0.10	0.13	5.6×10^{-3}	7.8×10^{-5}	1.6×10^{-6}
$t_{1/2}$, $ArNO_2$		1.2 min	4.5 min	3.5 min	74 min	3.8 day	90 day
LFER slope		0.08	0.14	0.11	0.22	0.20	0.42
^{15}N-AKIE ($\pm 1\sigma$)		1.0176 (0.0007)	1.0235 (0.0008)	n.d.[e]	1.0405 (0.0011)	1.0481 (0.0016)	n.d.

[a] Reduction potential of the half reaction $ArNO_2 + e^- = ArNO_2^{\bullet -}$ (*20*). [b] Duplicate reactors were used, with the average rate reported; agreement was generally within 10−15%. [c] $\sigma_x < 0.01$. [d] Data not shown in Figures 1 and 6 due to overlap with $x = 0.48$ (data shown in Figure S3). [e] Not determined due to lack of magnetite sample.

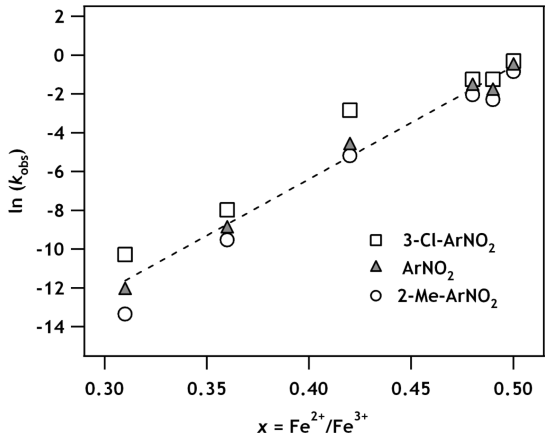

FIGURE 3. Natural log transformed observed kinetics for R-$ArNO_2$ compounds with different stoichiometry magnetites. The fitted line shown is for all R-$ArNO_2$ compounds vs x ($n = 15$; $R^2 = 0.96$).

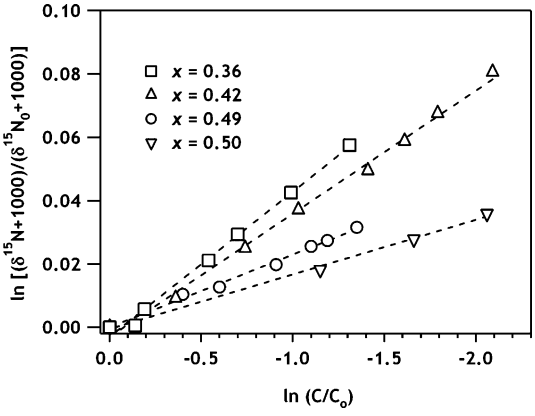

FIGURE 4. Linearized nitrogen isotope enrichment according to eq 2 during the reduction of $ArNO_2$ in suspension of magnetites with varying x. The slopes of the dashed lines correspond to bulk ^{15}N enrichment factors, ϵ_N, which, in the sequence of increasing x, were −17.2 ± 0.7‰, −23.0 ± 0.8‰, −39.0 ± 1.1‰, and −45.9 ± 1.6‰ ($\pm 1\sigma$). Error bars are smaller than the data markers. Legend: ▽ $x = 0.50$, ○ $x = 0.49$, △ $x = 0.42$, □ $x = 0.36$. Experimental conditions: 6.0 g/L magnetite, pH 7.2, 50 mM MOPS buffer, 1 h equilibration prior to addition of $ArNO_2$, $[ArNO_2]_0 = 400\ \mu M$.

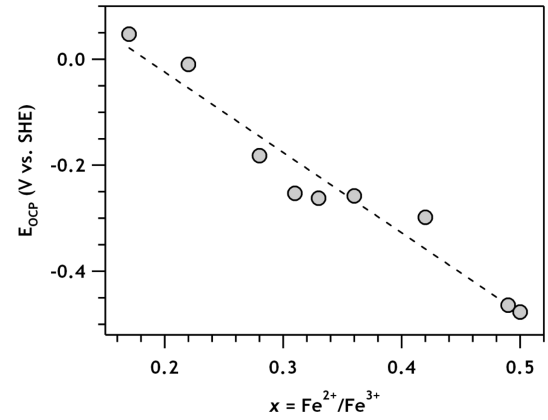

FIGURE 5. E_{OCP} of each magnetite batch plotted against the measured stoichiometry. The fitted linear regression with $n = 9$ yields $E(x) = [-1.52 \pm 0.14]x + [0.28 \pm 0.05]$ ($\pm\sigma$) vs SHE; $R^2 = 0.95$.

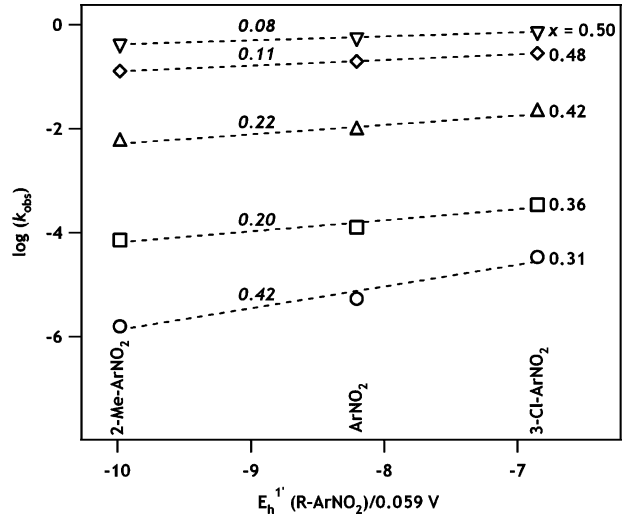

FIGURE 6. Linear free-energy relationship of magnetites with varying stoichiometries for three $ArNO_2$ analogs (3-Cl-$ArNO_2$, $ArNO_2$, 2-Me-$ArNO_2$). Legend: ▽ $x = 0.50$, ◇ $x = 0.48$, △ $x = 0.42$, □ $x = 0.36$, ○ $x = 0.31$. The values provided above the fitted lines are the LFER slopes. The data are also presented in Table 1.

−0.38 V (*15*) vs SHE), and we suspect that the range is due to differences in magnetite stoichiometry, which is rarely reported.

Substituent Effects on Rates of Nitrobenzene Reduction by Magnetite. To evaluate the effect of structural substituents on rates of $ArNO_2$ reduction by different stoichiometry magnetites, we plotted the log of reaction rates for substituted nitroaromatic compounds versus their $E_h^{1'}$ values (Figure 6). Although plots of $\log(k_{obs})$ versus $E_h^{1'}$ are typically considered linear free energy relationships (LFERs), recall that the ^{15}N-AKIE values indicate that cleavage of the first N−O bond, rather than electron transfer, may be the rate limiting step for the more oxidized magnetite samples, potentially making

$E_h^{1'}$ a less promising descriptor than it would be for a system where nitro reduction was entirely limited by the rate of electron transfer. The trends in slopes from the LFER plot are still nonetheless instructive to consider. The free energies of the first electron transfer ($E_h^{1'}$/0.059) cocorrelate with the overall rate of $ArNO_2$ reduction (*24*), and thus provide a qualitative means to assess the effects of contaminant structure on its reactivity (*27, 30*).

For the range of magnetite stoichiometries investigated, the LFER slopes are all less than 1 and decrease from 0.42 to 0.08 as the magnetite becomes more stoichiometric, indicating that the rates of $ArNO_2$ reduction by magnetite are affected by the contaminant's structure (substituent effects), and thus its electron-accepting properties. Shallower LFER slopes as the magnetite becomes more stoichiometric are consistent with the shift to lower ^{15}N-AKIE values shown in Figure 4, and provide additional evidence that a change in the rate-limiting step is occurring as the magnetite stoichiometry changes. LFER slopes significantly less than 1 have been reported for the reduction of other contaminants by Fe^{2+} associated with magnetite and other iron oxides, and have been interpreted to indicate transport limitations on the reaction rate (*36, 37*); however, as discussed above with regard to the shift to lower ^{15}N-AKIE values, we cannot distinguish whether the shallower LFER slopes observed for the more stoichiometric magnetite are due to a shift to a secondary reaction pathway (such as $e^-/e^-/H^+/H^+$ *22, 24*), or the onset of some transport limitation. Note that the LFER slopes including 2-Me-$ArNO_2$ may result in slightly underestimated slopes for $x = 0.31-0.42$ because 2-Me-$ArNO_2$ often reacts faster than predicted based on $E_h^{1'}$ values (*20, 31, 36*); the effect, however, would be identical for LFERs of all magnetite stoichiometries, and does not change the above interpretations.

Redox Behavior of Magnetite: Implications for Contaminant Reduction. Our findings that particle stoichiometry dramatically affects the reduction rates of monosubstituted nitrobenzene compounds have both fundamental and practical implications for understanding the redox behavior of magnetite with regard to contaminant fate. On a fundamental level, our work suggests that conceptual models for magnetite oxidation that rely solely on Fe^{2+} diffusion (*10−13*) or redox processes (*15*) may not be sufficient for describing contaminant reduction rates. Our ^{15}N-AKIE results indicate that transport limitations are not controlling the rate of $ArNO_2$ reduction by magnetite. This means that models based solely on diffusion, such as the core−shell diffusion model, where magnetite oxidation is limited by rates of Fe^{2+} migration from the core of the magnetite particle out through an oxidized maghemite shell (e.g,. (*11*)), are not applicable to contaminant reduction by magnetite. In addition, the strong linear correlation between E_{OCP} and magnetite stoichiometry (Figure 5) provides compelling evidence that redox processes play an important role in controlling rates of $ArNO_2$ reduction by magnetite. We propose that conceptual models that incorporate both redox and diffusion processes, such as those developed to describe magnetite oxidation and Fe^0 corrosion oxidation (*14, 15, 17, 18*), are more appropriate for understanding $ArNO_2$ reduction by magnetite. We suspect that this may be true for other contaminants as well (*16*).

On a more practical level, the strong correlation between magnetite stoichiometry and rates of $ArNO_2$ reduction (Figure 3) compelled us to explore whether a quantitative structure−activity relationship (QSAR) could be used to predict rates of $ArNO_2$ reduction (*21*). Magnetite stoichoimetry can be measured by complete dissolution and colorimetric measurements, and could potentially serve as an accessible descriptor variable for contaminant reduction rates. The relationship between E_{OCP} and x in Figure 5 can then be used to estimate the E_{OCP} as a function of magnetite stoichiometry. By taking the difference between the one-electron reduction potentials ($E_h^{1'}$) as a proxy for the redox activity for the substituted $ArNO_2$ compounds and E_{OCP}, we can approximate the overpotential (ΔE), or thermodynamic driving force using eq 3.

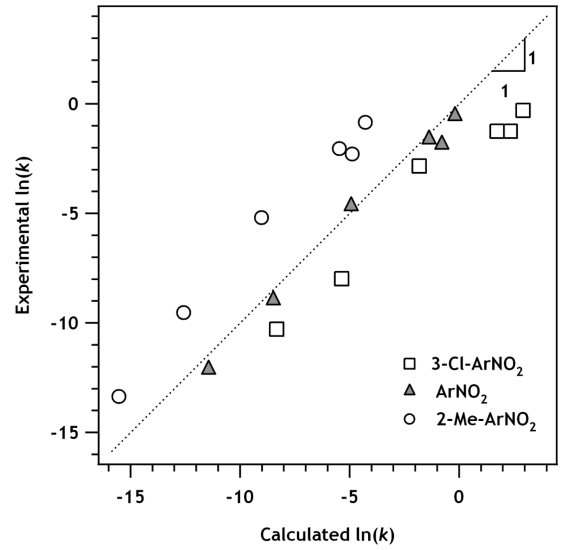

FIGURE 7. Comparison of experimentally measured k_{obs} values versus calculated k_{obs} values for R-$ArNO_2$ reduction by magnetites of varying stoichiometries. Experimental k_{obs} rates are the average of duplicate experiments. Calculated k_{obs} values were estimated from $E_h^{1'}$ values for R-$ArNO_2$ (Table 1) and E_{OCP} values for each magnetite stoichiometry (Table S1). An example calculation is provided in Supporting Information.

$$\Delta E(x) = E_h^{1'} - E_{OCP}(x) \quad (3)$$

In the absence of mass transfer effects, the overpotential can be used to estimate the rate of nitroaromatic reduction (calculation in Supporting Information). Figure 7 shows a comparison of the estimated rates and the experimentally measured rates. Agreement between the calculated and experimental values is quite good for $ArNO_2$ (within half an order of magnitude), but not as close for the two substituted $ArNO_2$ compounds (within 2 orders of magnitude). The QSAR systematically underpredicts the rate of 3-Cl-$ArNO_2$ and overpredicts the rate of 2-Me-$ArNO_2$, possibly due to mass transfers limitations or $E_h^{1'}$ not being an appropriate reaction descriptor. It is also possible that other thermodynamic values may prove to be better predictors of the reaction kinetics in the future (e.g., the bond dissociation enthalpy for the N−O cleavage) (*22*). Nonetheless, the QSAR may provide a useful tool for estimating rates of contaminant reduction by magnetite.

Acknowledgments

This work was supported by a National Science Foundation NIRT grant (EAR-0506679). T.B.H. acknowledges financial support from the Swiss NSF (200020-116447/1). We thank Jakov Bolotin for nitrogen isotope measurements.

Supporting Information Available

Figures displaying the raw kinetic data collected for all the substituted $ArNO_2$ compounds, E_{OCP} measurements for Figure 5, and a sample QSAR calculation. This information is available free of charge via the Internet at http://pubs.acs.org.

Literature Cited

(1) Cornell, R. M.; Schwertmann, U. *The Iron Oxides: Structure, Properties, Reactions, Occurrence, and Uses*; VCH: New York, 2003.

(2) Lippert, C. P. Big discovery for biogenic magnetite. *Proc. Natl. Acad. Sci. U. S. A.* **2008**, *105*, 17595–17596.
(3) Nagayama, M.; Cohen, M. The anodic oxidation of iron in neutral solution: 1. The nature and composition of the passive film. *J. Electrochem. Soc.* **1962**, *109*, 781–790.
(4) McCormick, M. L.; Bouwer, E. J.; Adriaens, P. Carbon tetrachloride transformation in a model iron-reducing culture: Relative kinetics of biotic and abiotic reactions. *Environ. Sci. Technol.* **2002**, *36*, 403–410.
(5) Tamaura, Y.; Ito, K.; Katsura, T. Transformation of γ-FeO(OH) to Fe_3O_4 by adsorption of iron(II) ion on γ-FeO(OH). *Chem. Soc. Dalton Trans.* **1983**, *2*, 189–194.
(6) Lee, W.; Batchelor, B. Abiotic reductive dechlorination of chlorinated ethylenes by iron-bearing soil minerals. 1. Pyrite and magnetite. *Environ. Sci. Technol.* **2002**, *36*, 5147–5154.
(7) Scott, T. B.; Allen, G. C.; Heard, P. J.; Randell, M. G. Reduction of U(VI) to U(IV) on the surface of magnetite. *Geochim. Cosmochim. Acta* **2005**, *69*, 5639–5646.
(8) White, A. F.; Peterson, M. L. Reduction of aqueous transition metal species on the surfaces of Fe(II)-containing oxides. *Geochim. Cosmochim. Acta* **1996**, *60*, 3799–3814.
(9) Gorski, C. A.; Scherer, M. M. Influence of magnetite stoichiometry on Fe^{II} uptake and nitrobenzene reduction. *Environ. Sci. Technol.* **2009**, *43*, 3675–3680.
(10) Gallagher, K. J.; Feitknecht, W.; Mannweiler, U. Mechanism of oxidation of magnetite to γ-Fe_2O_3. *Nature* **1968**, *217*, 1118–1121.
(11) White, A. F.; Peterson, M. L.; Hochella, M. F. Electrochemistry and dissolution kinetics of magnetite and ilmenite. *Geochim. Cosmochim. Acta* **1994**, *58*, 1859–1875.
(12) Sidhu, P. S.; Gilkes, R. J.; Posner, A. M. Mechanism of the low temperature oxidation of magnetite. *J. Inorg. Nucl. Chem.* **1977**, *39*, 1953–8.
(13) Tang, J.; Myers, M.; Bosnick, K. A.; Brus, L. E. Magnetite Fe_3O_4 nanocrystals: Spectroscopic observation of aqueous oxidation kinetics. *J. Phys. Chem. B* **2003**, *107*, 7501–7506.
(14) Chen, C.-T.; Cahan, B. D. The nature of the passive film on iron. I. Automatic ellipsometric spectroscopy studies. *J. Electrochem. Soc.* **1982**, *129*, 17–26.
(15) Castro, P. A.; Vago, E. R.; Calvo, E. J. Surface electrochemical transformations on spinel iron oxide electrodes in aqueous solutions. *J. Chem. Soc., Faraday Trans.* **1996**, *92*, 3371–3379.
(16) Vikesland, P. J.; Heathcock, A. M.; Rebodos, R. L.; Makus, K. E. Particle size and aggregation effects on magnetite reactivity toward carbon tetrachloride. *Environ. Sci. Technol.* **2007**, *41*, 5277–5283.
(17) Cahan, B. D.; Chen, C.-T. The nature of the passive film on iron. II. A-C impedance studies. *J. Electrochem. Soc.* **1982**, *129*, 474–480.
(18) Cahan, B. D.; Chen, C.-T. The nature of the passive film on iron. III. The chemi-conductor model and further supporting evidence. *J. Electrochem. Soc.* **1982**, *129*, 921–925.
(19) Stockbridge, C. D.; Sewell, P. B.; Cohen, M. Cathodic behavior of iron single crystals and the oxides Fe_3O_4 γ-Fe_2O_3, and α-Fe_2O_3. *J. Electrochem. Soc.* **1961**, *108*, 928–933.
(20) Schwarzenbach, R. P.; Stierli, R.; Lanz, K.; Zeyer, J. Quinone and iron porphyrin mediated reduction of nitroaromatic compounds in homogeneous aqueous solution. *Environ. Sci. Technol.* **1990**, *24*, 1566–1574.
(21) Tratnyek, P. G.; Weber, E. J.; Schwarzenbach, R. P. Quantitative structure-reactivity relationships for chemical reductions of organic contaminants. *Environ. Toxicol. Chem.* **2003**, *22*, 1733–1742.
(22) Colon, D.; Weber, E. J.; Anderson, J. L.; Suarez, L. A. Reduction of nitrosobenzenes and *N*-hydroxylanilines by Fe(II) species: Elucidation of the reaction mechanism. *Environ. Sci. Technol.* **2006**, *40*, 4449–4454.
(23) Haderlein, S.; Hofstetter, T.; Schwarzenbach, R. P., Subsurface chemistry of nitroaromatic compounds. In *Biodegradation of Nitroaromatic Compounds and Explosives*; Spain, J. C., Hughes, J. B., Knackmuss, H.-J., Eds.; Lewis Publishers: Boca Raton, FL, 2000; pp 311−357.
(24) Hartenbach, A. E.; Hofstetter, T. B.; Aeschbacher, M.; Sander, M.; Kim, D.; Strathmann, T. J.; Arnold, W. A.; Cramer, C. J.; Schwarzenbach, R. P. Variability of nitrogen isotope fractionation during the reduction of nitroaromatic compounds with dissolved reductants. *Environ. Sci. Technol.* **2008**, *42*, 8352–8359.
(25) Nurmi, J. T.; Bandstra, J. Z.; Tratnyek, P. G. Packed powder electrodes for characterizing the reactivity of granular iron in borate solutions. *J. Electrochem. Soc.* **2004**, *151*, B347–B353.
(26) Nurmi, J. T.; Tratnyek, P. G. Electrochemical studies of packed iron powder electrodes: Effects of common constituents of natural waters on corrosion potential. *Corros. Sci.* **2008**, *50*, 144–154.
(27) Hofstetter, T. B.; Neumann, A.; Arnold, W. A.; Hartenbach, A. E.; Bolotin, J.; Cramer, C. J.; Schwarzenbach, R. P. Substituent effects on nitrogen isotope fractionation during abiotic reduction of nitroaromatic compounds. *Environ. Sci. Technol.* **2008**, *42*, 1997–2003.
(28) Berg, M.; Bolotin, J.; Hofstetter, T. B. Compound-specific nitrogen and carbon isotope analysis of nitroaromatic compounds in aqueous samples using solid-phase microextraction coupled to GC/IRMS. *Anal. Chem.* **2007**, *79*, 2386–2393.
(29) Peterson, M. L.; Brown, G. E.; Parks, G. A. Direct XAFS evidence for heterogeneous redox reaction at the aqueous chromium/magnetite interface. *Colloids Surf., A* **1996**, *107*, 77–88.
(30) Neumann, A.; Hofstetter, T. B.; Skarpeli-Liati, M.; Schwarzenbach, R. P. Reduction of polychlorinated ethanes and carbon tetrachloride by structural Fe(II) in smectites. *Environ. Sci. Technol.* **2009**, *43*, 4082–4089.
(31) Neumann, A.; Hofstetter, T. B.; Lussi, M.; Cirpka, O. A.; Petit, S.; Schwarzenbach, R. P. Assessing the redox reactivity of structural iron in smectites using nitroaromatic compounds as kinetic probes. *Environ. Sci. Technol.* **2008**, *42*, 8381–8387.
(32) Danielsen, K. M.; Hayes, K. F. pH dependence of carbon tetrachloride reductive dechlorination by magnetite. *Environ. Sci. Technol.* **2004**, *38*, 4745–4752.
(33) Grygar, T. Dissolution of pure and substituted goethites controlled by the surface reaction under conditions of abrasive stripping voltammetry. *J. Solid State Electrochem.* **1997**, *1*, 77–82.
(34) Grygar, T.; Marken, F.; Schroder, U.; Scholz, F. Electrochemical analysis of solids. A review. *Collect. Czech. Chem. Commun.* **2002**, *67*, 163–208.
(35) Pang, S. C.; Chin, S. F.; Anderson, M. A. Redox equilibria of iron oxides in aqueous-based magnetite dispersions: Effect of pH and redox potential. *J. Colloid Interface Sci.* **2007**, *311*, 94–101.
(36) Klausen, J.; Trober, S. P.; Haderlein, S. B.; Schwarzenbach, R. P. Reduction of substituted nitrobenzenes by Fe(II) in aqueous mineral suspensions. *Environ. Sci. Technol.* **1995**, *29*, 2396–2404.
(37) Hofstetter, T. B.; Heijman, C. G.; Haderlein, S. B.; Holliger, C.; Schwarzenbach, R. P. Complete reduction of TNT and other (poly)nitroaromatic compounds under iron-reducting subsurface conditions. *Environ. Sci. Technol.* **1999**, *33*, 1479–1487.

ES9016848

SUPPORTING INFORMATION

Redox Behavior of Magnetite: Implications for Contaminant Reduction

Christopher A. Gorski[1], James T. Nurmi[2], Paul G. Tratnyek[2], Thomas B. Hofstetter[3], Michelle M. Scherer[1*]

[1]Civil and Environmental Engineering, University of Iowa, Iowa City, IA, 52240
[2]Dept. of Environmental Science and Engineering Oregon Graduate Institute of Science and Technology, Portland, OR, 97006
[3]Institute of Biogeochemistry and Pollutant Dynamics, Swiss Federal Institute of Technology (ETH) Zurich, Switzerland
[*]michelle-scherer@uiowa.edu

Instrument and chemical details contains information regarding the chemical vendor and purity, as well as details regarding the instrumentation used. **Table S1** contains the E_{OCP} data collected for magnetite batches with varying stoichiometries shown in Figure 5. **Figures S1 and S2** contain first-order reduction kinetics of substituted $ArNO_2$ compounds by magnetites with varying stoichiometries are shown for 2-Me-$ArNO_2$ and 3-Cl-$ArNO_2$, respectively. **Figure S3** contains all the kinetic experiments shown in Table 1 plotted as a function of stoichiometry. **Figure S4** is the measured open circuit potentials of magnetite-packed electrodes in pH 7.2, N_2-purged buffer. **Calculation S1** is an example calculation for equation 3 in the text used to produce Figure 7.

Instrument and chemical details

Chemicals used:

MOPS buffer: Research Product International Corporation, >99%
Ferrous chloride (anyhydrous): Fisher Scientific, 99.99%
Ferric chloride (anhydrous, lump): Fisher Scientific, >97%
H_2O_2: Fisher Scientific, 30%
Methanol: Burdick and Jackson, >99.9%
Aniline, Fisher Scientific, 99.9%
Nitrobenzene, Fisher Scientific, 99.9%
2-Me-Aniline, Acros Organics, 99%
2-Me-Nitrobenzene, Acros Organics, 99%
3-Cl-Aniline, Acros Organics, 99%
3-Cl-Nitrobenzene, Acros Organics, 98%

Instruments used:

TEM: Joel 1230 TEM
pXRD: Rigaku Miniflex II, equipped with a Co source
^{57}Fe Mössbauer spectrometer: 13 K He system equipped with a ~30 mCu ^{57}Co source from Science Engineering and Education Co.
HPLC: Agilent 1100 Series HPLC
BET: Automated surface area analyzer, Quantachrome BET Nova 4200e

Table S1. Measured E_{OCP} of magnetites with varying stoichiometries after 60 minutes equilibration; data shown in **Figure 5**. Measurements reported are of single specimens; when sufficient material was available, duplicate E_{OCP} measurements were done, and the results generally agreed within 5%. $\sigma_x < 0.01$ for all batches.

$x = Fe^{2+}/Fe^{3+}$	E_{OCP}[a] (V vs. SHE)
0.50	-0.477
0.49	-0.464
0.42	-0.298
0.36	-0.258
0.31	-0.253
0.28	-0.182
0.33	-0.262
0.22	-0.010
0.17	+0.047

[a] Open-circuit potential.

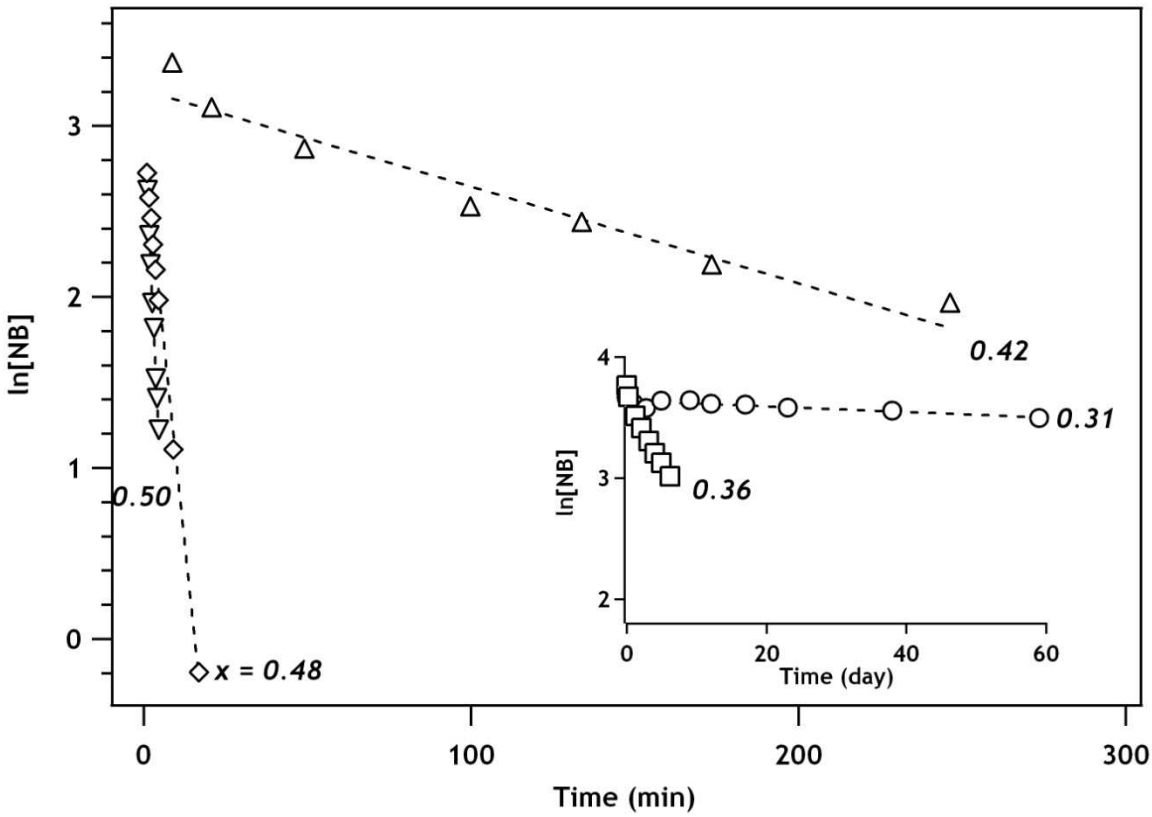

Figure S1. First-order plot for 2-Me-$ArNO_2$ reduction by magnetite with different stoichiometries (x = Fe^{2+}/Fe^{3+}). Legend: ▽ x = 0.50, ◇ x = 0.48, △ x = 0.42, □ x = 0.36, ○ x = 0.31. Experimental conditions: 1 g/L magnetite, pH 7.2, 50 mM MOPS buffer, 1 hour equilibration prior to addition of 2-Me-$ArNO_2$, [2-Me-$ArNO_2$]$_0$ = 40 μM.

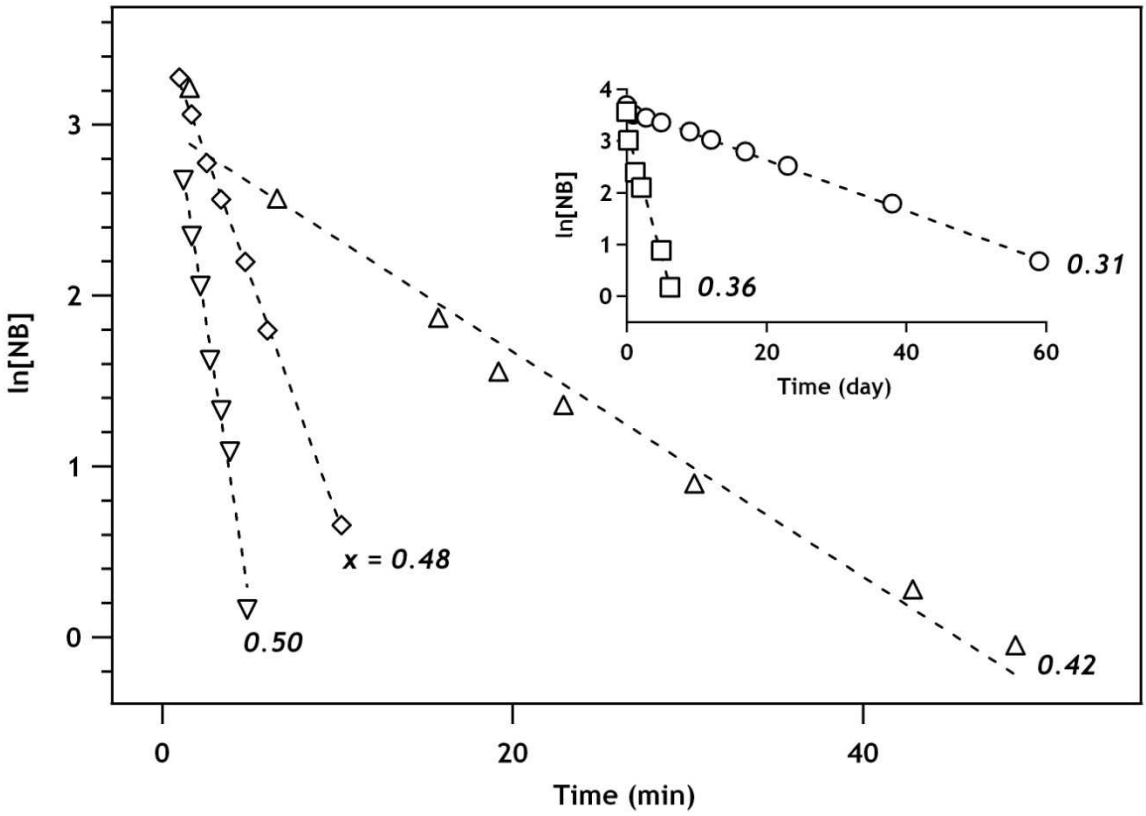

Figure S2. First-order plot for 3-Cl-$ArNO_2$ reduction by magnetite with different stoichiometries (x = Fe^{2+}/Fe^{3+}). Legend: ▽ x = 0.50, ◇ x = 0.48, △ x = 0.42, □ x = 0.36, ○ x = 0.31. Experimental conditions: 1 g/L magnetite, pH 7.2, 50 mM MOPS buffer, 1 hour equilibration prior to addition of 3-Cl-$ArNO_2$, [3-Cl-$ArNO_2$]$_0$ = 40 µM.

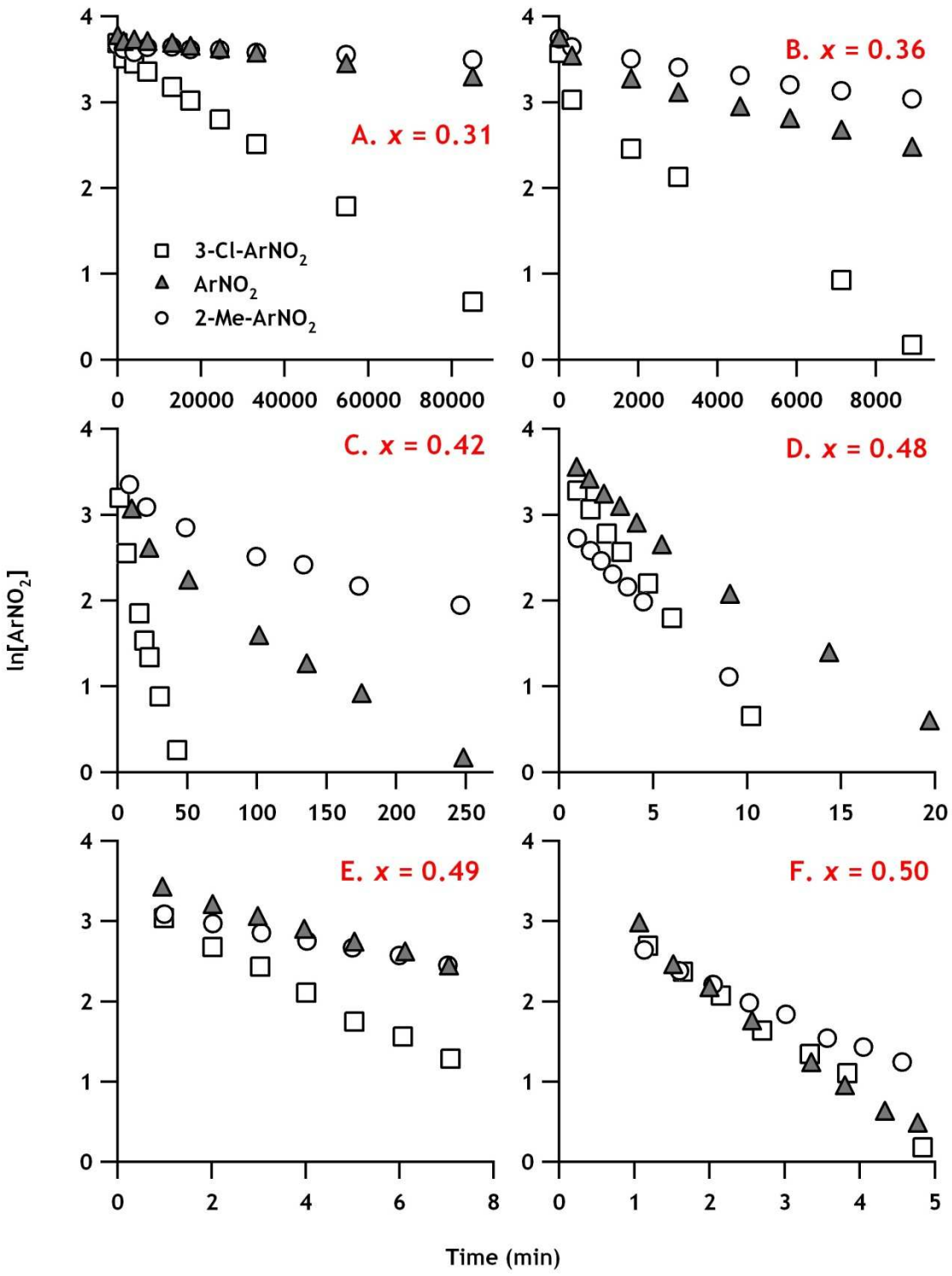

Figure S3. First-order kinetics of substituted nitrobenzene compounds by magnetites of varying stoichiometries (x = Fe^{2+}/Fe^{3+}). Experimental conditions: pH 7.2, 50 mM MOPS, 1 g/L magnetite, 40 µM nitrobenzene. First-order linear fits are presented in Table 1.

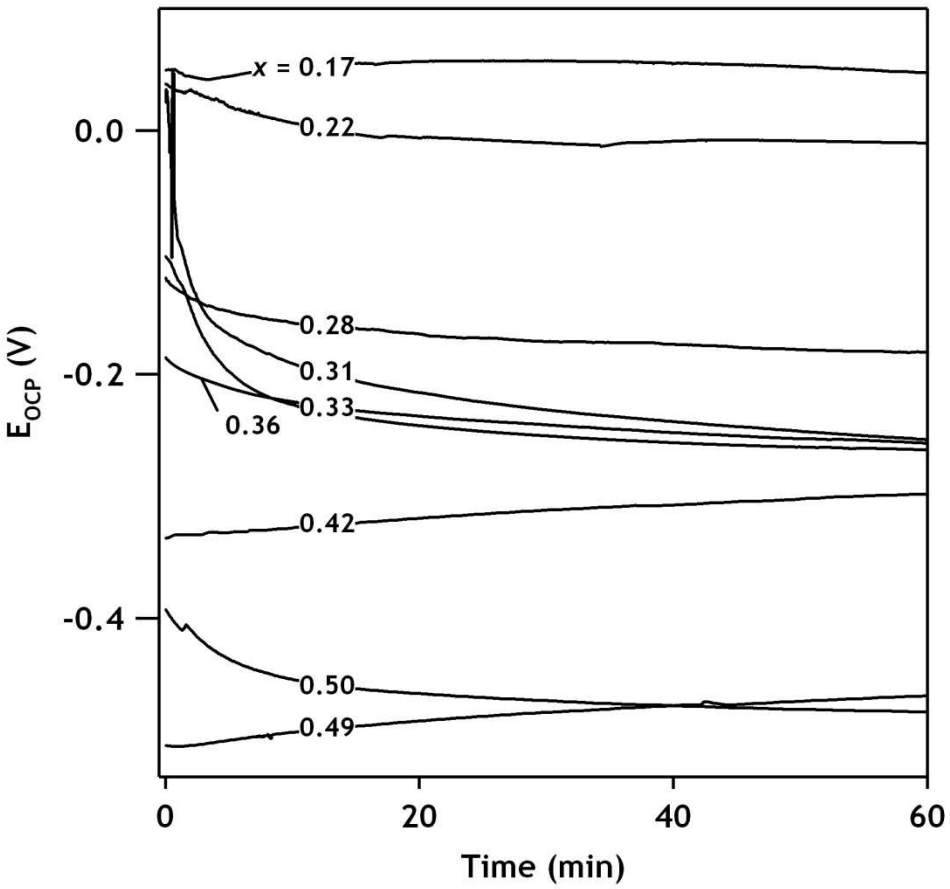

Figure S4. The measured open-circuit potentials (E_{OCP}) of magnetite-packed electrodes in N_2 purged 50 mM MOPS, pH 7.2. The written values on the figure are the stoichiometry ($x = Fe^{2+}/Fe^{3+}$) for each sample. Values shown are in reference to SHE.

Calculation S1. Production of the calculated rates in Figure 7 of the main text.

Example calculation for $ArNO_2$ reduction by magnetite. Note for substituted nitroaromatics (or other contaminants), $E_h^{1'}$ will be the only variable that changes; thus, the y-intercept will shift, but the slope will still be dependent only on $E_{OCP}(x)$.

$$\mathbf{E_{cell}}(x) = E_h^{1'} - \mathrm{E_{OCP}}(x)$$

For $ArNO_2$: ($E_h^{1'}$ = -0.485 V)

$$\mathbf{E_{cell}}(x) = [-0.485\ V — (-1.52(x) + 0.28\ \mathrm{V})]$$

$$\mathbf{E_{cell}}(x) = [-0.765\ V + 1.52(x)]$$

$$\ln[k(x)] = \alpha\frac{-nF}{RT}[\mathrm{E_{cell}}(x)] + \beta$$

n = 1; F = 96.485 kC; R = Ideal gas constant, T = absolute temperature (298 K here)

Assume α = 1 (adiabatic); β = 0 (allow E_a to determine intercept)

$$\ln[k(x)] = -29.8 + 59.2(x)$$